AIAA JOURNAL
Vol. 31, No. 9, September 1993

Updating Finite Element Dynamic Models Using an Element-by-Element Sensitivity Methodology

Charbel Farhat* and Francois M. Hemez†
University of Colorado, Boulder, Colorado 80309

A sensitivity-based methodology for improving the finite element model of a given structure using test modal data and a few sensors is presented. The proposed method searches for both the location and sources of the mass and stiffness errors and does not interfere with the theory behind the finite element model while correcting these errors. The updating algorithm is derived from the unconstrained minimization of the squared $\mathcal{L}_2$ norms of the modal dynamic residuals via an iterative two-step staggered procedure. At each iteration, the measured mode shapes are first expanded assuming that the model is error free, then the model parameters are corrected assuming that the expanded mode shapes are exact. The numerical algorithm is implemented in an element-by-element fashion and is capable of "zooming" on the detected error locations. Several simulation examples which demonstrate the potential of the proposed methodology are discussed.

I. Introduction

EVEN though the field of finite element analysis of structural dynamic problems has witnessed tremendous progress in the last two decades, greater confidence is still placed in experimental data. Therefore, the finite element model of a given structure is often updated to reflect the results of a particular experiment. Usually, the computed eigenmodes are compared with the measured frequencies and mode shapes. If both sets are not in agreement, the finite element model is refined via a two-step updating procedure which: 1) locates the errors and 2) corrects them. Clearly, the first step is the most challenging of the two. Once the location of the errors is known, it is relatively easy to correct them, especially if the error sources can be identified. However, locating and identifying these errors can be a difficult task for the following reasons. In general, only a few experimental modes are available, and these may be contaminated with random and systematic measuring errors. Moreover, only a subset of the degrees of freedom (DOF) in the finite element model can be monitored; and as for practical and economical reasons, only a few sensors can be utilized.

Many updating procedures have been proposed in recent years, each with its own advantages and shortcomings due to the different limitations and assumptions. A class of methods using Lagrange multipliers was initially developed by Baruch,[1] Berman and Nagy,[2] and Caesar.[3] Matrix adjustment procedures have been presented by Kabe[4] and Smith and Beattie,[5] and direct methods based on matrix perturbation have been proposed by Chen et al.[6] Statistics and sensitivity methods have been investigated, among others, by Collins et al.,[7] Chen and Wada,[8] Lallement and Piranda,[9] and Lallement and Zhang.[10] Methods based on force balance have been proposed by Berger et al.[11] and by Ojalvo and Pilon.[12] Updating techniques using frequency response data and a combination of modal and frequency response data were proposed by Mottershead[13] and Creamer and Junkins.[14] Various substructure-by-substructure (SBS) and element-by-element (EBE) computational procedures for model updating have been developed by Berger et al.[15] and recently by Bernitsas and Tawekal,[16] to name only a couple. Complete reviews of this growing field can be found in the recent literature by Ibrahim and Saafan,[17] Caesar,[18] and Heylen and Sas.[19]

Here, we present a sensitivity-based EBE (SB-EBE) method for improving the finite element model of a given structure using test modal data. The proposed method searches for both the location and potential sources of the detected errors and does not interfere with the theory behind the finite element model while correcting these errors. It is described in great detail in the subsequent sections, which are organized as follows. Section II presents the overall SB-EBE method for the case where only the stiffness matrix needs to be corrected. The case where both the mass and stiffness matrices need to be refined is treated in Sec. III. Section IV addresses the "zooming" properties and computational aspects of the SB-EBE method and Sec. V illustrates the proposed procedure with simulation examples. Finally, Sec. VI addresses orthogonality issues, and Sec. VII concludes this paper.

II. Sensitivity-Based Element-by-Element Updating Procedure

A. Physical Approach to the Updating Problem

We consider an undamped structural model. First, we assume that its mass matrix does not need any adjustment. The simultaneous updating of the mass and stiffness matrices is dealt with in Sec. III. The notation used throughout this paper employs the superscripts $()^E$, $()^A$, and $()^U$ to denote experimental (measured), analytical (finite element), and updated values, respectively, and the subscripts $()_M$ and $()_{NM}$ to label the measured and nonmeasured DOF in the given finite element model, respectively. The analytical mass and stiffness matrices satisfy

$$K^A V_r^A = M^A V_r^A \Omega_r^A \tag{1}$$

where r denotes the number of available experimental modes. In general, the experimental and finite element data are in disagreement, so that

$$\Omega_r^A \neq \Omega_r^E; \qquad V_r^A \neq V_r^E \tag{2}$$

$$K^A V_r^E \neq M^A V_r^E \Omega_r^E \tag{3}$$

As written Eq. (3) assumes that the analytical and experimental models have the same size, although in most practical cases, the number of DOF in the finite element model exceeds by far the number of measured ones. Moreover, unless special

Received Feb. 6, 1992; revision received Feb. 19, 1993; accepted for publication March 10, 1993.

*Associate Professor, Department of Aerospace Engineering Sciences, Center for Space Structures and Controls and Center for Space Construction. Senior Member AIAA.

†Research Assistant, Department of Aerospace Engineering Sciences, Center for Space Structures and Controls and Center for Space Construction. Member AIAA.

care has been taken, the measured DOF do not necessarily coincide with those of the discrete mesh. One possible way to overcome this difficulty is to choose the measured DOF as masters and reduce the size of the finite element model via a matrix condensation technique (see, for example, Guyan[20] and Paz[21]). Here, we have decided not to explore this avenue, mainly because all reduction techniques yield matrices where the connectivity of the original finite element model is destroyed, and thus the physical meaning of that model is lost. Rather we have opted for an augmentation technique where the measured mode shapes are expanded to the size of the analytical ones. A review and comparison of some of the previously proposed expansion methods can be found in Gysin's work.[22]

First, we define the augmented experimental mode shapes where V^E_{rM} and V^E_{rNM} represent the measured (instrumented) and nonmeasured components of r experimental mode shapes, respectively,

$$\bar{V}^E_r = \begin{bmatrix} V^E_{rM} \\ V^E_{rNM} \end{bmatrix}$$

The objective of any stiffness updating procedure is to construct a matrix $K^U = K^A + \Delta K$ such that

$$K^U \bar{V}^E_r = M^A \bar{V}^E_r \Omega^E_r \tag{4}$$

The preceding system of equations where ΔK and V^E_{rNM} are the fundamental unknowns is, in general, rectangular, thus a more appropriate formulation of the updating problem is given by:

find ΔK and V^E_{rNM} such that $\|(K^U - \omega_i^{E2} M^A)\bar{v}^E_i\|_2$ is minimized

$$\text{for } i = 1, 2, \ldots, r \tag{5}$$

However, whatever system of equations arises from the preceding formulation, its algebraic solution is of little interest because it fails to directly answer two fundamental questions: what are the errors and where are they located. Moreover, as formulated in Eq. (5), the updating problem may yield a stiffness matrix K^U where the original connectivity of the finite element model is destroyed. However, we note that there exists in the literature direct matrix updating algorithms in which the original connectivity of the structure is maintained (see, for example, Refs. 4 and 5). In this work, we assume that the mathematical theory of the given finite element model is sound and that eventual errors found in the correlation between the analytical and experimental results are mainly due to an imperfect knowledge of some important parameters of the structure, such as its material and geometrical properties, and/or to an inaccurate representation of structural joints and boundary conditions. These sources of error can be traced at the element level of the model. Therefore, we express ΔK as

$$\Delta K = \sum_{e=1}^{e=n_e} \Delta K^{(e)} \tag{6}$$

where n_e denotes the total number of elements in the mesh. We expand $\Delta K^{(e)}$ as

$$\Delta K^{(e)} = K^{(e)}(p_1 + \delta p_1, \ldots, p_{n_p} + \delta p_{n_p}) - K^{(e)}(p_1, \ldots, p_{n_p}) \approx \sum_{k=1}^{k=n_p} \frac{\partial K^{(e)}}{\partial p_k} \delta p_k \tag{7}$$

where p_k denotes a generic parameter of a structural element such as its Young modulus E, its Poisson ratio ν, its cross-sectional area A, its thickness t, or its moment of inertia around a y axis I_y, and n_p denotes the total number of parameters characterizing a given element level stiffness matrix. Wherever $K^{(e)}$ is a linear function of a parameter p_k, the expansion (7) can handle arbitrarily large parameter perturbations δp_k. However, when $K^{(e)}$ is a higher order or transcendental function of p_k, only small perturbations δp_k should be considered in principle. Each matrix $\partial K^{(e)}/\partial p_k$ describes the sensitivity of the element level stiffness matrix to a variation in parameter p_k. Examples of sensitivity matrices are given in Appendix A. In the remainder of this paper, we use the simplified notation:

$$s^{(e)}_k = \frac{\partial K^{(e)}}{\partial p_k} \tag{8}$$

Next, we introduce the following r functionals:

$$J_i(v^E_{iNM}, p_1, \ldots, p_{n_p \times n_e}) = \bar{v}_i^{E^t} \left(\sum_{e=1}^{e=n_e} \left[K^{(e)} + \sum_{k=1}^{k=n_p} s^{(e)}_k \delta p_k \right] - \omega_i^{E2} M^{(e)} \right)^t \left(\sum_{e=1}^{e=n_e} \left[K^{(e)} + \sum_{k=1}^{k=n_p} s^{(e)}_k \delta p_k \right] - \omega_i^{E2} M^{(e)} \right) \bar{v}^E_i \tag{9}$$

for $i = 1, 2, \ldots, r$. Each functional J_i is the square of the $\mathcal{L}_2$ norm of the ith modal dynamic residual

$$R_i = (K^U - \omega_i^{E2} M^A)\bar{v}^E_i \tag{10}$$

Using Eqs. (6–9), the updating problem (5) is transformed into

find $(\delta p_1, \ldots, \delta p_{n_p \times n_e})$ and V^E_{rNM} such that J_i is minimized

$$\text{for } i = 1, 2, \ldots, r \tag{11}$$

which physically corresponds to the minimization of the modal dynamic residuals. In general, the second variation of each J_i is not positive. Therefore, for all practical purposes, a local minimum for Eq. (11) is sought after via the solution of

$$\begin{aligned} &\frac{\partial J_i}{\partial \delta p_k} = 0 && k = 1, 2, \ldots, n_p \times n_e \\ &&& i = 1, 2, \ldots, r \\ &\frac{\partial J_i}{\partial v^E_{iNM}} = 0 && i = 1, 2, \ldots, r \end{aligned} \tag{12}$$

Equations (12) lead to a complex nonlinear system in the physical parameters and the nonmeasured DOF that is difficult to solve with conventional methods. Here, we seek a solution of Eqs. (12) via the following iterative algorithm which can be interpreted as a linearization procedure: Given $\delta p^0_k = 0$, $k = 1, 2, \ldots, n_p \times n_e$; for $n = 1, 2, \ldots$, until convergence:

Step 1) Solve

$$\frac{\partial J_i}{\partial v^E_{iNM}}(v^{En}_{iNM}, \delta p^{n-1}_k) = 0 \text{ for } i = 1, 2, \ldots, r$$

Step 2) Compute the new modal dynamic residuals using v^{En}_{iNM}.

Step 3) Solve

$$\frac{\partial J_i}{\partial \delta p_k}(v^{En}_{iNM}, \delta p^n_k) = 0$$

$$\text{for } k = 1, 2, \ldots, n_p \times n_e \text{ and } i = 1, 2, \ldots, r$$

Step 4) Update:

$$K^{Un} = \sum_{e=1}^{e=n_e} \left[K^{(e)} + \sum_{k=1}^{k=n_p} s^{(e)}_k \delta p^n_k \right] = K^{Un-1} + \sum_{e=1}^{e=n_e} \left[\sum_{k=1}^{k=n_p} s^{(e)}_k \bar{\delta} p^n_k \right] \tag{13}$$

$$\delta p^n_k = \delta p^{n-1}_k + \bar{\delta} p^n_k \qquad k = 1, 2, \ldots, n_p \times n_e$$

Step 5) Check convergence.

Basically, each iteration is a two-step staggered procedure. First, the measured mode shapes are expanded assuming that

the model is error free (step 1). Next, the model parameters are corrected assuming that the expanded mode shapes are exact (step 3). The updating algorithm yields a modified stiffness matrix K^{Un} which has the same connectivity and the same rigid-body modes as the original finite element stiffness matrix. Moreover, the overall procedure does not interfere with the underlying finite element "technology" (element derivation and properties).

B. Mode Expansion

If the updated stiffness matrix K^U is partitioned as

$$K^U = \begin{bmatrix} K^U_{M,M} & K^U_{M,NM} \\ K^U_{NM,M} & K^U_{NM,NM} \end{bmatrix} \tag{14}$$

and the original analytical mass matrix is partitioned in the same fashion, then at each iteration n, step 1 yields for each experimental mode the following system of linear equations:

$$A_i^n v_{iNM}^{En} = -b_i^n \qquad \text{for } i = 1, 2, \ldots, r \tag{15}$$

where

$$\begin{aligned} A_i^n &= [Z_{iNM,NM}^{Un-1}]^t [Z_{iNM,NM}^{Un-1}] + [Z_{iM,NM}^{Un-1}]^t [Z_{iM,NM}^{Un-1}] \\ b_i^n &= \left[[Z_{iNM,NM}^{Un-1}]^t [Z_{iM,NM}^{Un-1}]^t + [Z_{iM,NM}^{Un-1}]^t [Z_{iM,M}^{Un-1}] \right] v_{iM}^E \end{aligned} \tag{16}$$

The ith impedance matrix at iteration n, Z_i^{Un}, is defined as $Z_i^{Un} = K^{Un} - \omega_i^{E2} M^{An}$ and partitioned in the same fashion as the stiffness matrix (14). For each mode i, A_i^n is a square matrix whose size is equal to the number of nonmeasured DOF and has full rank. The solution of the corresponding system (15) fully determines the ith mode expansion.

C. Updating the Physical Parameters

The correction of the physical parameters p_k is performed in step 3 of Eq. (13) which yields the following algebraic linear system:

$$[B^{nt} B^n] \bar{\delta} p^n = -B^{nt} R_r^{n-1} \tag{17}$$

where

$$B^n = \begin{bmatrix} [s_1^{(1)} L^{(1)} \bar{v}_1^E] & \cdots & [s_{n_p}^{(n_e)} L^{(n_e)} \bar{v}_1^E] \\ [s_1^{(1)} L^{(1)} \bar{v}_2^E] & \cdots & [s_{n_p}^{(n_e)} L^{(n_e)} \bar{v}_2^E] \\ \vdots & \ddots & \vdots \\ [s_1^{(1)} L^{(1)} \bar{v}_r^E] & \cdots & [s_{n_p}^{(n_e)} L^{(n_e)} \bar{v}_r^E] \end{bmatrix} \tag{18}$$

and

$$\bar{\delta} p^n = [\bar{\delta} p_1^{(1)} \cdots \bar{\delta} p_{n_p}^{(1)} \cdots \bar{\delta} p_{n_p}^{(n_e)}]^t \tag{19}$$

The localization operator $L^{(e)}$ extracts from a given vector those DOF which are attached to the nodal points of finite element e. The matrix product $[B^{nt} B^n]$ is $(n_e \times n_p) \times (n_e \times n_p)$ and has full rank. However, a much smaller system needs to be solved in practice, as discussed in Sec. IV.

III. Simultaneous Updating of the Mass and Stiffness Matrices

Here we consider the case where both the mass and stiffness matrices need to be updated. The errors in M^A are monitored at the element level

$$\Delta M = \sum_{e=1}^{e=n_e} \Delta M^{(e)} \tag{20}$$

The sensitivity of every element level mass matrix to a variation in a parameter p_k can be written as

$$t_k^{(e)} = \frac{\partial M^{(e)}}{\partial p_k} \tag{21}$$

and a first-order Taylor expansion of $\Delta M^{(e)}$ leads to

$$\Delta M^{(e)} \approx \sum_{k=1}^{k=m_p} t_k^{(e)} \delta p_k \tag{22}$$

where p_k now denotes a generic parameter characterizing the element level mass and stiffness matrices such as the density ρ or the Young modulus E, and where m_p denotes the total number of parameters characterizing an element level mass matrix. The stiffness and mass parameters are not necessarily the same, and n_p is not necessarily equal to m_p. The r functionals introduced in Eq. (9) are now defined as

$$\begin{aligned} J_i(v_{iNM}^E, p_1, \ldots, p_{l_p \times n_e}) = \bar{v}_i^{Et} \Bigg(& \sum_{e=1}^{e=n_e} K^{(e)} - \omega_i^{E2} M^{(e)} \\ & + \left[\sum_{k=1}^{k=n_p} s_k^{(e)} \delta p_k - \omega_i^{E2} \sum_{q=1}^{q=m_p} t_q^{(e)} \delta p_q \right] \Bigg)^t \Bigg(\sum_{e=1}^{e=n_e} K^{(e)} - \omega_i^{E2} M^{(e)} \\ & + \left[\sum_{k=1}^{k=n_p} s_k^{(e)} \delta p_k - \omega_i^{E2} \sum_{q=1}^{q=m_p} t_q^{(e)} \delta p_q \right] \Bigg) \bar{v}_i^E \end{aligned} \tag{23}$$

for $i = 1, 2, \ldots, r$ and where l_p denotes the maximum number of parameters characterizing a pair $\{M^{(e)}, K^{(e)}\}$. The updating algorithm is similar to that expressed in Eq. (13). At each iteration n, the mass matrix and physical parameters are updated as

$$\begin{aligned} M^{Un} &= \sum_{e=1}^{e=n_e} \left[M^{(e)} + \sum_{k=1}^{k=m_p} t_k^{(e)} \delta p_k^n \right] = M^{Un-1} + \sum_{e=1}^{e=n_e} \left[\sum_{k=1}^{k=m_p} t_k^{(e)} \bar{\delta} p_k^n \right] \\ \delta p_k^n &= \delta p_k^{n-1} + \bar{\delta} p_k^n \qquad k = 1, 2, \ldots, m_p \times n_e \end{aligned} \tag{24}$$

The mode expansion phase results in a linear system of equations that is similar to Eq. (15) after replacing M^A with M^U. Now, the first of Eqs. (12) leads to

$$[B^{nt} B^n] \bar{\delta} p^n = -B^{nt} R_r^{n-1} \tag{25}$$

where

$$B^n = \begin{bmatrix} [d_{1,1}^{(1)} L^{(1)} \bar{v}_1^E] & \cdots & [d_{l_p,1}^{(n_e)} L^{(n_e)} \bar{v}_1^E] \\ [d_{1,2}^{(1)} L^{(1)} \bar{v}_2^E] & \cdots & [d_{l_p,2}^{(n_e)} L^{(n_e)} \bar{v}_2^E] \\ \vdots & \ddots & \vdots \\ [d_{1,r}^{(1)} L^{(1)} \bar{v}_r^E] & \cdots & [d_{l_p,r}^{(n_e)} L^{(n_e)} \bar{v}_r^E] \end{bmatrix} \tag{26}$$

with

$$\bar{\delta} p^n = [\bar{\delta} p_1^{(1)} \cdots \bar{\delta} p_{l_p}^{(1)} \cdots \bar{\delta} p_{l_p}^{(n_e)}]^t \tag{27}$$

and $d_{k,i}^{(e)} = (s_k^{(e)} - \omega_i^{E2} t_k^{(e)})$. Upon convergence, the solution of Eq. (25) provides the set of corrected parameters p_k. The notation implies that some sensitivities may be zero, for example, if a given element level matrix does not depend on a specific parameter. The matrix product $[B^{nt} B^n]$ is at most $(n_e \times l_p) \times (n_e \times l_p)$ and has full rank. However, as mentioned earlier, a much smaller system needs to be solved in practice.

IV. Zooming Properties and Computational Aspects

A. Locating and Identifying the Errors

In most practical cases, the finite element modeling errors are concentrated in some areas of the discrete mesh. Therefore, it is essential to design an updating algorithm which can zoom on these error locations. Otherwise, much of the computer CPU time would be spent trying to correct error-free components of the finite element model.

The reader should recall that the correction of the physical parameters is performed in step 3 of the updating algorithm (13) and is given by the solution of the following linear system:

$$[B^{nt}B^n]\bar{\delta}p^n = -B^{nt}R_r^{n-1}$$

Therefore, one may reasonably expect that the only elements that need to contribute to the left-hand side $[B^{nt}B^n]$, that is, the only elements that need to be corrected at iteration n will be those which are connected to degrees of freedom where the right-hand side $B^{nt}R_r^{n-1}$ is relatively important, that is, where the modal dynamic residuals are the largest. The latter criterion is known as the modal force error criterion[11,12]; it has recently been shown to be a useful indicator for damage detection.[23] The details of the zooming procedure are as follows. Let Ω^n denote the set of global DOF where a modal dynamic residual exceeds at iteration n a certain limit l_R

$$|[R_i^n]_j| = |[(K^{Un} - \omega_i^{E2}M^{Un})\bar{v}_i^{En}]_j| \geq l_R \tag{28}$$

for $i = 1, 2, \ldots, r$. In this work, l_R is established via a statistical procedure applied to the components of the vectors R_i^n, $i = 1, 2, \ldots, r$ (see Appendix B). A reasonable location of the modeling errors is given by $\bar{\Omega}^n$, the set of elements that are connected to the DOF listed in Ω^n. If $\bar{n}_e^n$ denotes the total number of elements in $\bar{\Omega}^n$, then only the fundamental parameters of $\bar{n}_e^n$ elements need to be updated at iteration n. Practically, only a few parameters need to be updated within each element of $\bar{\Omega}^n$. At each iteration n, the set of these parameters is denoted by $\mathcal{P}^n$ and is constructed as follows. First, for every measured mode, the partial variations of its corresponding localized residual are computed with respect to all parameters p_k

$$\frac{\partial L^{(e)}R_i^n}{\partial p_k} = d_{k,i}^{(e)n}L^{(e)}\bar{v}_i^{En}$$
$$\text{for } k = 1, 2, \ldots, l_p \quad \text{and} \quad i = 1, 2, \ldots, r \tag{29}$$

Next, the parameters to be updated at iteration n in a given element are selected as those which result in the largest values of

$$\|d_k^{(e)n}\| = \sum_{i=1}^{i=r} \|d_{k,i}^{(e)n}L^{(e)}\bar{v}_i^{En}\|_2 \times |\bar{\delta}p_k^{n-1}| \tag{30}$$

that is, those parameters for which one has

$$\|d_k^{(e)n}\| \geq l_d \tag{31}$$

and where the threshold l_d is evaluated using the same statistical procedure as for l_R (see Appendix B). In summary, if $\bar{l}_p^n$ denotes the total number of parameters in the finite element model to be corrected at iteration n, we expect for most problems where modeling errors are localized to have

$$\bar{n}_e^n \ll n_e$$
$$\bar{l}_p^n \ll n_e \times l_p \tag{32}$$

The simulation examples discussed in Sec. V substantiate this claim.

B. Computational Issues

At each iteration n, the correction of the physical parameters p_k requires that B^n [Eq. (26)] be re-evaluated and $[B^{nt}B^n]$ be refactored. This does not come as a surprise, since the original updating problem [Eqs. (11) and (12)] is a nonlinear one. However, for all practical purposes, the size of the matrix product $[B^{nt}B^n]$ is $\bar{l}_p^n \times \bar{l}_p^n$, which is, as discussed earlier, much smaller than the theoretical size $(n_e \times l_p) \times (n_e \times l_p)$. Therefore, it is computationally feasible to setup and solve at each iteration the system of linear equations (25). Because $[B^{nt}B^n]$ is typically ill-conditioned, the singular value decomposition (SVD) algorithm[24] is used to solve Eqs. (25) rewritten as $B^n\bar{\delta}p^n = -R_r^{n-1}$. If n_M and n_N denote the total number of measured DOF and the total number of nonmeasured DOF, respectively, and if a pair of $(+, \times)$ is counted as one floating-point operation (FLOP), the cost of solving Eq. (25) via the SVD algorithm and without zooming is:

$$\text{FLOP} = 3 \times r \times (n_M + n_N) \times (n_p \times n_e)^2 + 10 \times (n_p \times n_e)^3 \tag{33}$$

With zooming, this cost reduces to

$$\text{FLOP} = 3 \times r \times (n_M + n_N) \times \bar{l}_p^{n2} + 10 \times \bar{l}_p^{n3} \tag{34}$$

The other component of the updating algorithm (13) corresponds to the expansion of the measured mode shapes. The computations associated with this phase deserve special attention. Let $Z_{iM,NM}$ and $Z_{iNM,NM}$ be defined as follows:

$$Z_{iM,NM} = (K_{M,NM}^{Un-1} - \omega_i^{E2}M_{M,NM}^{Un-1})$$
$$Z_{iNM,NM} = (K_{NM,NM}^{Un-1} - \omega_i^{E2}M_{NM,NM}^{Un-1}) \tag{35}$$

After replacing M^A with M^U, the system of equations (15) which governs the mode expansion phase at each iteration n can be written as:

$$A_i^n = [Z_{iNM,NM}]^t[Z_{iNM,NM}^t] + [Z_{iM,NM}]^t[Z_{iM,M}] \tag{36}$$

Clearly, whether a lumped or consistent mass formulation is used in the finite element model, $Z_{iM,NM}$ and $Z_{iNM,NM}$ have the same sparsity pattern as $K_{M,NM}^U$ and $K_{NM,NM}^U$, respectively, but the matrix quantity $[Z_{iNM,NM}^t Z_{iNM,NM} + Z_{iM,NM}^t Z_{iM,NM}]$ offers no structure to be exploited. Therefore, computing explicitly the left-hand side of Eq. (15) destroys the sparsity patterns of the building blocks $Z_{iM,NM}$ and $Z_{iNM,NM}$. For this reason, the solution of Eq. (15) is not computed via the explicit evaluation and factorization of the sum of the matrix products $[Z_{iNM,NM}^t Z_{iNM,NM} + Z_{iM,NM}^t Z_{iM,NM}]$, but via the procedure outlined subsequently. Using the Woodbury formula,[25] the solution of Eq. (15) can be written as

$$v_{iNM}^{En} = [D^{-1} - D^{-1}E^t(I + ED^{-1}E^t)^{-1}ED^{-1}]b_i^n \tag{37}$$

where $D = Z_{iNM,NM}^t Z_{iNM,NM}$ and $E = Z_{iM,NM}$. Note that all of D, E, and $I + ED^{-1}E^t$ are symmetric positive matrices. In particular, $Z_{iNM,NM}$ can be factored as

$$Z_{iNM,NM} = CC^t \tag{38}$$

where C and C^t are the lower- and upper-triangular Cholesky factors, respectively. Therefore, D can be written as

$$D = CC^tCC^t \tag{39}$$

Given an arbitrary vector y, a matrix-vector product of the form $x = D^{-1}y$ can be implemented as the solution of the following lower- and upper-triangular systems

$$\begin{aligned} &\text{lower solve:} && C\bar{x} = y \\ &\text{upper solve:} && C^t\tilde{x} = \bar{x} \\ &\text{lower solve:} && Cx^* = \tilde{x} \\ &\text{upper solve:} && C^tx = x^* \end{aligned} \tag{40}$$

Since $K_{NM,NM}$ is sparse and usually stored in a skyline form, the Cholesky factor C inherits the same skyline pattern as $K_{NM,NM}$. In the sequel, we denote by b the semibandwidth (or average column height) of $K_{NM,NM}$. On the other hand, the matrix quantity $I + ED^{-1}E^t$ is explicitly assembled and factored as

$$I + ED^{-1}E^t = C^*C^{*t} \tag{41}$$

where the superscript asterisk is used to differentiate between the Cholesky factors of $I + ED^{-1}E^t$ and those of $Z_{iNM,NM}$ of Eq. (38). In general, the matrix $I + ED^{-1}E^t$ is full. However, $I + ED^{-1}E^t$ is only $n_M \times n_M$. As a typical value of n_M in a modal test is 200 (162 for the Galileo spacecraft[26]), it is therefore computationally feasible to store and factor $I + ED^{-1}E^t$. In summary, the ith expanded mode shape v_{iNM}^{En} can be computed as follows [we indicate between parenthesis the computational complexity of each step in terms of floating-point operations (+ , ×)]:

factor:	$(n_N \times b^2/2)$	$Z_{iNM,NM} = CC^t$
factor:	$(n_M^3/6)$	$I + ED^{-1}E^t = C^*C^{*t}$
solve:	$(2 \times n_N \times b)$	$Dz = b_i^n$
multiply:	$(2 \times n_N \times c_{M,NM})$	$\bar{z} = Ez$
solve:	(n_M^2)	$C^*C^{*t}\bar{z} = \bar{z}$
multiply:	$(2 \times n_M \times c_{M,NM})$	$z^* = E^t\bar{z}$
solve:	$(2 \times n_N \times b)$	$Dy = z^*$
final solution:	(n_N)	$v_{iNM}^{En} = z - y$ (42)

In the preceding expressions, $c_{M,NM}$ denotes the average number of nonmeasured DOF that are connected in the finite element model to a given measured DOF and therefore can be bounded by

$$c_{M,NM} < b \tag{43}$$

The total computational complexity of the computational scheme is

$$\text{FLOP} = n_N \times (b^2/2 + 4 \times b + 1) + n_M \times (n_M^2/6 + n_M + 4 \times c_{M,NM}) \tag{44}$$

For large structures, the computational cost is of the order of $n_N \times b^2/2$ and, therefore, is less than the cost of factoring the finite element global stiffness matrix K.

V. Applications

Four simulation examples are reported here, each illustrating the behavior of the proposed updating algorithm for a different problem. In the remainder of this section, the "experimental" model is represented by the unperturbed finite element model. The "analytical" model is represented by the perturbed finite element model and designated with the superscript ( )$^{(ana)}$. For every case, the measured results are simulated with the trace on a few degrees of freedom, of the numerical results associated with the unperturbed finite element model, and the analytical results are those computed using the perturbed finite element model. All computations are carried out on a Sun 4/260 workstation.

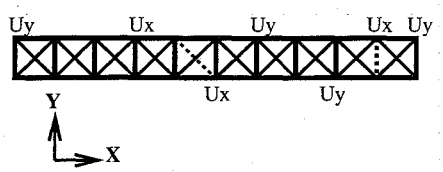

Fig. 1 Two-dimensional floating truss structure and its measured degrees of freedom, problem Sec. V.A.

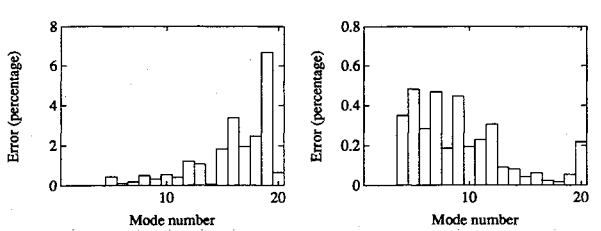

Fig. 2 Relative frequency errors before and after updating, problem Sec. V.A.

A. Local Stiffness Perturbations

Here, we consider a two-dimensional "floating" truss structure (Fig. 1) with 51 truss members, each with a Young modulus $E = 4.0 \times 10^7$ psi, and a cross-sectional area $A = 1.0$ in.^{2}. The corresponding finite element linear undamped model contains 44 DOF, of which seven DOF are assumed to be measured: three horizontal and four vertical displacements, at randomly selected nodes. The Young moduli of the two truss members 24 and 46 (shown dashed in Fig. 1) are perturbed and set to

$$\begin{cases} E_{24}^{(ana)} = 6.0 \times 10^7 \text{ psi} \\ E_{46}^{(ana)} = 2.0 \times 10^7 \text{ psi} \end{cases} \tag{45}$$

These large perturbations, + 30% and − 100% for E_{24} and E_{46}, respectively, are allowable because the stiffness matrix of a truss element is a linear function of E. The first eight modes (three rigid and five deformable) are assumed available for updating the finite element model. The frequency errors in-

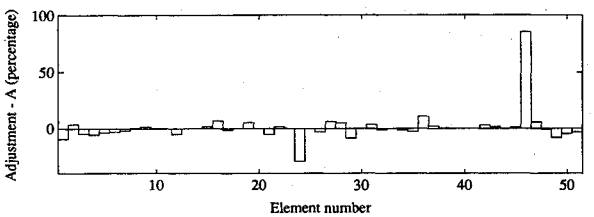

Fig. 3 Adjusted cross-sectional areas, problem Sec. V.A.

Table 1 Updating history (problem Sec. V.A)

Iteration	List of corrected parameters[a]	Size
1	A_{26} E_{26} A_{22} E_{22} A_{27} E_{27} A_{24} E_{24} A_{25} E_{25}	10
2	A_{46} E_{46} A_{43} E_{43} A_{49} E_{49} A_{44} E_{44} A_{45} E_{45}	10
3	A_{48} E_{48} A_{42} E_{42} A_{47} E_{47} A_{50} E_{50} A_{46} E_{46}	10
4	A_{46}	1
5	A_{29} E_{29} A_{28} E_{28} A_{30} E_{30} A_{24} A_{25} A_{26}	9
6	A_{23} E_{23} A_{24} A_{46} A_{26} A_{30} A_{42}	7
7	A_{14} E_{14} A_{16} E_{16} A_{46} A_{24} A_{42}	7
8	A_{18} E_{18} A_{13} E_{13} A_{25} A_{24}	6
9	A_{19} E_{19} A_{24} A_{13} A_{26} A_{23}	6
10	A_{21} E_{21} A_{20} E_{20} A_{13} A_{25} A_{23} A_{14} A_{28}	9
11	A_{24} A_{25} A_{13} A_{23}	4
12	A_{25} A_{42} A_{14} A_{23} A_{28}	5
13	A_{46} A_{24} A_{25}	3
14	A_{25} A_{13} A_{14} A_{23} A_{21} A_{28}	6
15	A_{24} A_{25}	2
16	A_{24} A_{25}	2
17	A_{25} A_{13} A_{14} A_{23}	4
18	A_{24} A_{25}	2
19	A_{44} A_{25} A_{42}	3
20	A_{24} A_{25}	2
21	A_{46} A_{25} A_{44}	3
22	A_{24} A_{25}	2
23	A_{24} A_{25}	2
24	A_{24} A_{25}	2
25	A_{24} A_{25}	2
26	A_{25} A_{24} A_{44} A_{23}	4
27	A_{41} E_{41} A_{25} A_{44} A_{23}	5
28	A_{25} A_{24} A_{44}	3
29	A_{46} A_{25} A_{41}	3
30	A_{24} A_{25}	2

[a]Boldface type is used to designate parameters belonging to actually perturbed elements.

Table 2 CPU requirements (problem Sec. V.A)

	With zooming	Without zooming
Maximum number of adjusted parameters per iteration	10	102
Number of iterations	100	100
Expansion phase Eq. (15)		
CPU time per iteration and per mode, s	0.13	0.13
CPU time per iteration and for the eight modes, s	1.01	1.02
Correction phase Eq. (25)		
CPU time per iteration, s	0.13	33.72
Total CPU time per iteration, s	1.50	36.11

Table 3 CPU requirements (problem Sec. V.B)

	Without zooming
Maximum number of adjusted parameters per iteration	100
Number of iterations	50
Expansion phase Eq. (15)	
CPU time per iteration and per mode, s	0.29
CPU time per iteration and for the five modes, s	1.43
Correction phase Eq. (25)	
CPU time per iteration, s	1.29
Total CPU time per iteration, s	3.34

duced by these perturbations are depicted in Fig. 2, before and after updating.

After 50 iterations, the updating algorithm reduces the frequency errors from a maximum relative error of 7% to a maximum relative error of 0.5%. However, as we have stressed earlier in this paper, it is also desirable that an updating algorithm be able to find both the location and source of a modeling error. Figure 3, which reports the adjusted cross-sectional areas in the analytical model, clearly demonstrates that our updating algorithm has located the perturbed members 24 and 46. Unfortunately, the cross-sectional areas of these members rather than their Young moduli are corrected here. The reason is that the "effective" parameter of $K^{(e)}$ is neither E nor A but the homogeneous product $E \times A$, so that the updating algorithm cannot distinguish in this case between E and A. However, this ambiguity is easily resolved in the presence of combined axial and bending deformations as will be illustrated in the following example (see problem V.B).

Table 1 lists the parameters that are adjusted during the first 30 iterations of the updating procedure with zooming. One can observe that the number of retained parameters rapidly decreases as the iteration count increases. It should be noted that because the modal force error criterion (28) is DOF based, whereas the zooming procedure is element based, all elements connected to a retained DOF in Ω^n are automatically selected in $\hat{\Omega}^n$, whether they need correction or not. For example, element 25, which is connected to element 24, is more often selected than the perturbed elements 24 and 46. However, element 25 is not corrected (see Fig. 3). Overall, the algorithm effectively zooms on the structural members 24 and 46. To highlight the computational savings due to the zooming procedure, the problem is repeated with the zooming capability disabled. As a result, all of the 102 parameters E and A are corrected at each iteration. Table 2 contrasts the CPU requirements for both solutions.

B. Global Stiffness Perturbation

In the preceding problem, the errors introduced in the finite element model are of a local nature since only two members are perturbed. However, a finite element model may be corrupted by global modeling errors due to manufacturing tolerances in geometrical and/or material properties. This section illustrates the performance of the proposed updating procedure in the presence of such modeling errors.

A given cantilever beam with a cross-sectional area $A = 2.5$ in.^{2} and a Young modulus $E = 10^5$ psi is discretized using 20 Euler-Bernouilli two-dimensional beam elements. The finite element model contains 60 DOF (40 translational, 20 rotational), of which eight translational DOF are assumed to be measured (Fig. 4). A systematic manufacturing error is here simulated by setting all the Young moduli to $E_1^{(ana)} = \cdots = E_{20}^{(ana)} = 99{,}000$ psi (-1% relative error). To reproduce realistic modal test conditions, only the five lowest modes are assumed to be available for updating.

After updating, the frequencies are greatly improved and all Young moduli are almost equally adjusted by $+1\%$. The corrections performed by the updating procedure on all of the other parameters are relatively negligible. Since each finite element in this model accounts for both bending stiffnesses $E \times I_z$ and axial stiffnesses $E \times A$, the updating algorithm is capable of distinguishing between errors in A and E. Note also that the adjustments shown in Fig. 5 are more accurate in finite elements 1–6 than they are in the other elements. This is

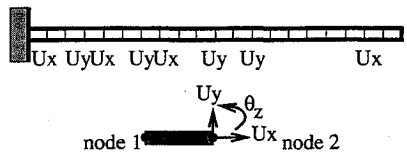

Fig. 4 Discretization and measured degrees of freedom, problem Sec. V.B.

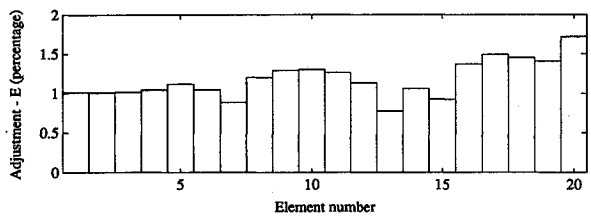

Fig. 5 Adjusted Young moduli, problem Sec. V.B.

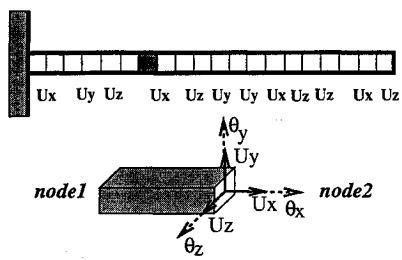

Fig. 6 Discretization and measured degrees of freedom, problem Sec. V.C.

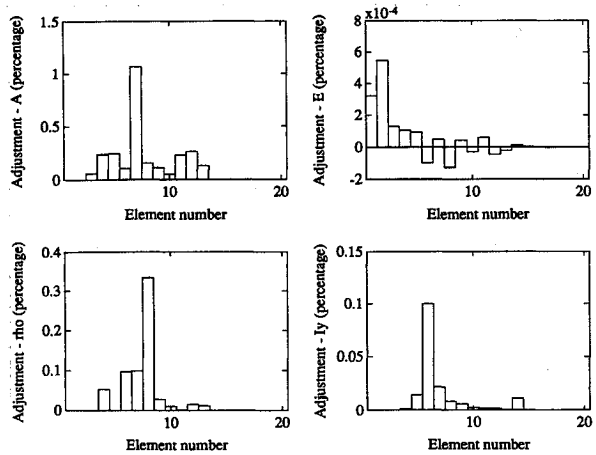

Fig. 7 Adjusted cross-sectional areas, Young moduli, densities, and y moments of inertia, problem Sec. V.C.

because elements 1–6 are located closer to the root of the cantilever beam and therefore store a higher percentage of the strain energy which make them highly "observable" by the updating algorithm. The CPU requirements for this simulation example are summarized in Table 3.

C. Local Stiffness and Mass Perturbations

The previous cantilever beam is here modeled as a three-dimensional structure. The corresponding finite element model contains 120 DOF (60 translational, 60 rotational) of which 12 translational DOF are assumed to be measured (Fig. 6). Only the five lowest modes are used in the updating algorithm. The cross-sectional area of element 7 (shown dashed in Fig. 6) is perturbed and set to $A_7^{(\text{ana})} = 2.475$ in.^{2}. This -1% level perturbation induces errors in both the stiffness and mass matrices. The adjustments of the cross-sectional areas A, the Young moduli E, the densities ρ, and the moment of inertia I_y are reported in Fig. 7; $I_y = I_z$ for this symmetric beam. The peak in Fig. 7 (cross-sectional areas) clearly demonstrates that the updating algorithm has found both the location and source of the modeling error. Even though E, ρ, and I_y are not perturbed in this example, the Young moduli, densities, and moments of inertia of a few members are shown to be slightly altered. This is a side effect of the proposed updating methodology. However, these modifications are negligible when compared to the adjustment of the cross-sectional area of element 7.

In problem V.B, the beam is represented with a two-dimensional finite element model where the sensitivity matrix $\partial K^{(e)}/\partial A$ is a linear function of the cross-sectional area A. Here, the beam is represented with a three-dimensional finite element model where, because of torsional effects, $\partial K^{(e)}/\partial A$ is a nonlinear function of A (see Appendix A). Consequently, Eq. (7) in this case contains a truncation error. However, this does not seem to upset the overall performance of the updating algorithm. The problem here is repeated with a -70% level perturbation in the cross-sectional area of element 7 so that the linearization implied by Eq. (7) is far from being satisfied. Surprisingly, the updating algorithm converges in only nine iterations (recall that it took 50 iterations for the -1% level perturbation in A_7) and recovers the -70% error in A_7 (Fig. 8). The faster convergence in the latter case can be

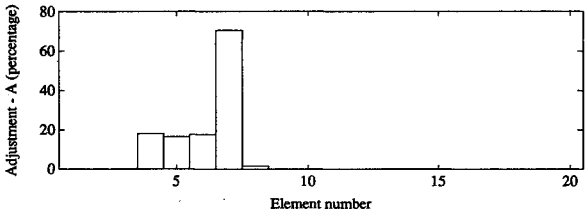

Fig. 8 Adjusted cross-sectional areas, problem Sec. V.C, − 70% error in A_7.

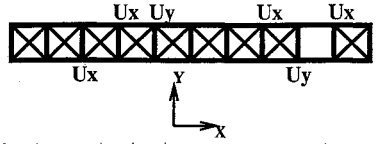

Fig. 9 Damaged truss structure and measured degrees of freedom, problem Sec. V.D.

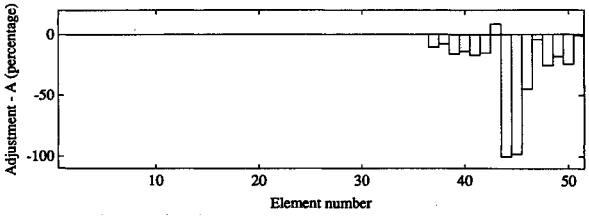

Fig. 10 Adjusted cross-sectional areas, problem Sec. V.D.

Table 4 CPU requirements (problem Sec. V.D)

	With zooming
Maximum number of adjusted parameters per iteration	30
Number of iterations	20
Expansion phase Eq. (15)	
CPU time per iteration and per mode, s	0.13
CPU time per iteration and for the eight modes, s	1.06
Correction phase Eq. (25)	
CPU time per iteration, s	0.56
Total CPU time per iteration, s	1.96

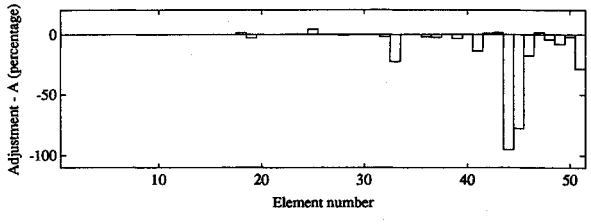

Fig. 11 Adjusted cross-sectional areas, problem Sec. V.D, redefined sensor locations.

simply explained by the fact that a 70% error in the cross-sectional area of a member is more "visible" by the algorithm than a 1% error because it leads to greater modal force errors [Eq. (28)].

D. Finding Missing Members

Finally, we consider the case where the two members 44 and 45 are removed from the "floating" truss structure described in Sec. V.A. The resulting perturbed structure is shown in Fig. 9, together with the six measured DOF (out of 44 DOF). Here, the updating is based on seven modes: the three rigid-body modes, the first two bending modes, and two higher order modes (the eighth and ninth flexible modes). Note that this means that nine modes are assumed to be available. The reason behind this specific selection of the measured modes is explained later. Removing the two diagonals in the ninth bay introduces an extra rigid-body mode; however, it does not interfere with the updating methodology.

After 20 iterations, the updating algorithm predicts a 100% reduction in the cross-sectional areas of members 44 and 45. This reduction affects both the stiffness and mass of these two truss members and clearly reveals the damage location (Fig. 10). For this simulation example, which illustrates the potential of the proposed methodology for identifying structural damage, the CPU time per iteration is roughly equally split between the mode expansion and parameter correction phases (Table 4). The cumulated CPU time for the expansion phase during the 20 iterations necessary for convergence is 21.16 s. As a reference, it takes 17.45 s for the subspace iteration algorithm to compute 20 modes for this structure.

In this example, two of the six sensors were coincidentally located at "damaged" degrees of freedom (see Fig. 9). Therefore, the problem was repeated after moving those two sensors to the right end of the truss so that no sensor measures directly a damaged DOF. Still, the updating algorithm converged in 19 iterations and pointed to members 44 and 45 as the missing members (Fig. 11). The strain energy distribution across the truss members for flexible modes 1–4, 8, and 9 is reported in Fig. 12. The pair of damaged members 44 and 45 are labeled with the letter D. Figure 12 shows that, for this particular problem, the damaged members are somehow "observable" by modes 1 and 2, highly observable by modes 8 and 9, but almost nonobservable by modes 3 and 4, which do not produce enough strain energy in the damaged members. We believe that this concept of observability is important for almost all modal-based updating methodologies. For example, if we had based our updating methodology on the three rigid modes

and flexible modes 1–4, we would have obtained the adjusted cross-sectional areas depicted in Fig. 13, which clearly point to member 45 as a missing member, but point to a lesser extent to member 44 as a missing member. Of course, the location of the damaged members is not known in advance in practice. However, the preceding example highlights the importance of the proper selection of the "measured" modes.

VI. Expansion and Orthogonality

After a given finite element model is updated, two sets of mode shapes are available where $i = 1, 2, \ldots, r$: 1) the expanded mode shapes $\bar{v}_i^E$ given by step 1 of the updating algorithm (13) upon convergence and 2) the mode shapes of the "truth" model $v_i^{(\text{truth})}$. For the previous simulation examples, the truth models correspond to the unperturbed models. For consistency, it is desirable that the two sets of modes be as close as possible, which implies a high level of accuracy in the expansion procedure. To this effect, the relative errors between these two mode sets here are measured as

$$\epsilon_i(\bar{v}_i^E, v_i^{(\text{truth})}) = \left| \frac{\|\bar{v}_i^E\|_2 - \|v_i^{(\text{truth})}\|_2}{\|\bar{v}_i^E\|_2} \right| \quad \text{for } i = 1, 2, \ldots, r \quad (46)$$

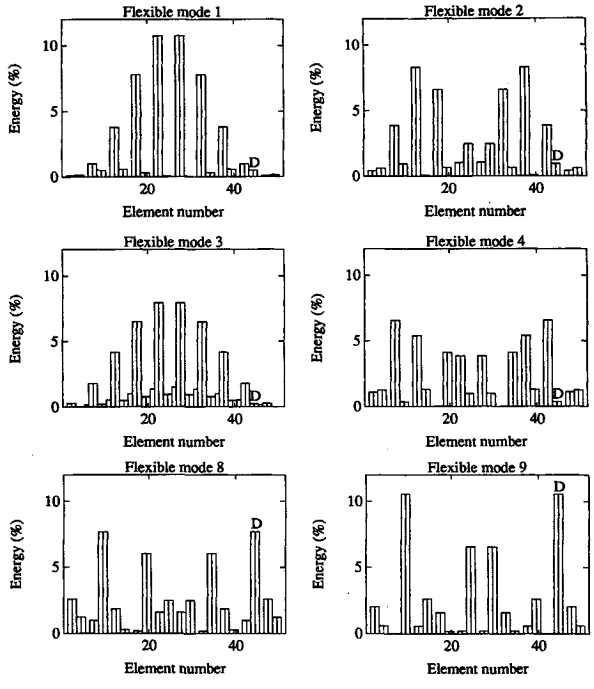

Fig. 12 Strain energy distribution, problem Sec. V.D.

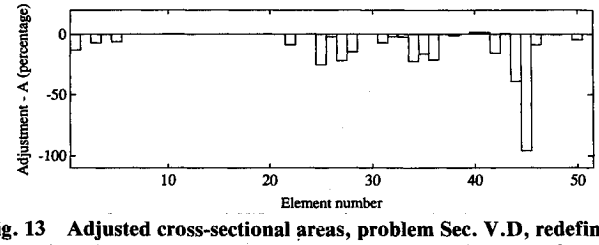

Fig. 13 Adjusted cross-sectional areas, problem Sec. V.D, redefined sensor locations, and based on the three rigid modes and flexible modes 1–4.

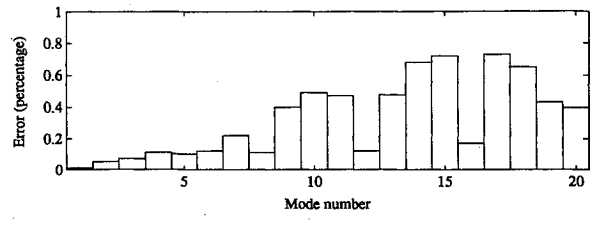

Fig. 14 Relative expansion errors, problem Sec. V.B.

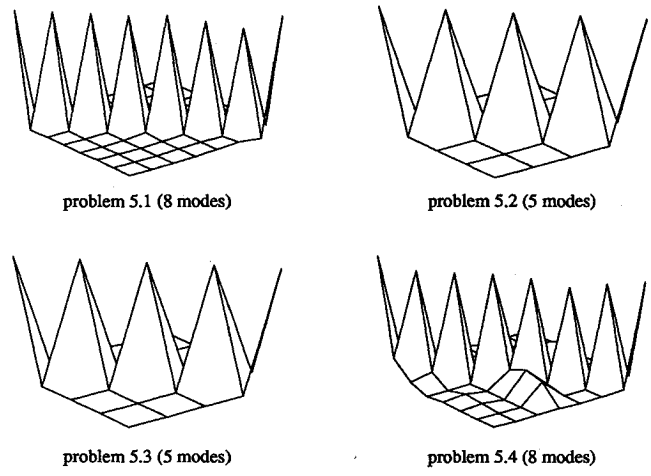

Fig. 15 Mass orthonormality of expanded mode shapes, problems Sec. V.A–V.D.

and reported in Fig. 14 for problem V.B. For all of the first 20 modes, these errors are less than 1%, which indicates high levels of consistency and accuracy of the expansion procedure. It should also be noted that, unlike other updating methodologies which are based on constrained minimization formulations (see, for example, Refs. 4 and 5), the proposed updating procedure is formulated as an unconstrained minimization problem (11) which does not explicitly reinforce the mass and stiffness orthogonality of the expanded mode shapes. However, these orthogonality conditions are implicitly embedded in the minimization formulation which, upon convergence, delivers the updated mass and stiffness matrices as well as their corresponding eigenvectors. This is illustrated in Fig. 15 which graphically depicts the coefficients of the product $\bar{V}_r^{Et} M^U \bar{V}_r^E$ associated with problems V.A–V.D. All diagonal terms are shown to be almost equal to one, and all off-diagonal coefficients are shown to be almost zero.

VII. Closure

A sensitivity-based methodology for improving the finite element model of a given structure using incomplete test modal data is presented. The proposed method searches for all of the location and physical sources of the mass and stiffness errors. Therefore, structural element properties and boundary conditions are corrected rather than matrix coefficients. The updating algorithm is derived from the unconstrained minimization of the $\mathcal{L}_2$ norms of the modal dynamic residuals via an iterative two-step staggered procedure. At each iteration, the measured mode shapes are first expanded assuming that the model is error free, then the model parameters are corrected assuming that the expanded mode shapes are exact. Upon convergence, the expansion procedure is shown to deliver consistent modal shapes that are orthonormal with respect to the updated stiffness and mass matrices, respectively. The parameter correlation allows large perturbations when the element level mass and/or stiffness matrices are linear functions of these parameters. The overall numerical algorithm is implemented in an element-by-element fashion with a zooming capability on detected errors. Several simulation examples are presented and discussed. These illustrate the performance of the proposed methodology and its potential for detecting modeling errors and structural damage.

Appendix A: Sensitivity Matrices for the Euler-Bernouilli Beam

Here we consider the case of a three-dimensional Euler-Bernouilli beam element where the degrees of freedom are ordered as

$$[v_{x1}\, v_{y1}\, v_{z1}\, \theta_{x1}\, \theta_{y1}\, \theta_{z1}\, v_{x2}\, v_{y2}\, v_{z2}\, \theta_{x2}\, \theta_{y2}\, \theta_{z2}] \quad (A1)$$

Table A1 Coefficients of the sensitivity matrices with respect to E and A

Coefficient	Derivative w.r.t. E	Derivative w.r.t. A
α	A/L	E/L
β_y	I_y	0
β_z	I_z	0
γ	$\dfrac{A^2}{4\times\pi\times L\times(1+\nu)}$	$\dfrac{E\times A}{2\times\pi\times L\times(1+\nu)}$
m_v	0	$\rho\times L/2$
m_θ	0	$\rho\times L^3/24$

Table A2 Coefficients of the sensitivity matrices with respect to ν, I_y, I_z, and ρ

Coefficient	Derivative w.r.t. ν	Derivative w.r.t. I_y	Derivative w.r.t. I_z	Derivative w.r.t. ρ
α	0	0	0	0
β_y	0	E	0	0
β_z	0	0	E	0
γ	$\dfrac{-E\times A^2}{4\times\pi\times L\times(1+\nu)^2}$	0	0	0
m_v	0	0	0	$A\times L/2$
m_θ	0	0	0	$A\times L^3/24$

The subscripts $()_1$ and $()_2$ refer to the two nodes of the element, and v and θ denote the displacement and rotation fields, respectively. The element level lumped mass matrix is given by Eq. (A4) and a corresponding stiffness matrix is given by Eq. (A5) where

$$m_v = \frac{\rho\times A\times L}{2} \qquad m_\theta = \frac{\rho\times A\times L^3}{24} \tag{A2}$$

and

$$\alpha = \frac{E\times A}{L} \qquad \beta_z = E\times I_z \qquad \beta_y = E\times I_y \qquad \gamma = \frac{E\times A^2}{[4\times\pi\times L\times(1+\nu)]} \tag{A3}$$

$$M^{(e)} = \text{diag}[m_v\ m_v\ m_v\ m_\theta\ m_\theta\ m_\theta\ m_v\ m_v\ m_v\ m_\theta\ m_\theta\ m_\theta] \tag{A4}$$

$$K^{(e)} = \begin{bmatrix}
\alpha & 0 & 0 & 0 & 0 & 0 & -\alpha & 0 & 0 & 0 & 0 & 0 \\
0 & \frac{12\beta_z}{L^3} & 0 & 0 & 0 & \frac{6\beta_z}{L^2} & 0 & -\frac{12\beta_z}{L^3} & 0 & 0 & 0 & \frac{6\beta_z}{L^2} \\
0 & 0 & \frac{12\beta_y}{L^3} & 0 & -\frac{6\beta_y}{L^2} & 0 & 0 & 0 & -\frac{12\beta_y}{L^3} & 0 & -\frac{6\beta_y}{L^2} & 0 \\
0 & 0 & 0 & \gamma & 0 & 0 & 0 & 0 & 0 & -\gamma & 0 & 0 \\
0 & 0 & -\frac{6\beta_y}{L^2} & 0 & \frac{4\beta_y}{L} & 0 & 0 & 0 & \frac{6\beta_y}{L^2} & 0 & \frac{2\beta_y}{L} & 0 \\
0 & \frac{6\beta_z}{L^2} & 0 & 0 & 0 & \frac{4\beta_z}{L} & 0 & -\frac{6\beta_z}{L^2} & 0 & 0 & 0 & \frac{2\beta_z}{L} \\
-\alpha & 0 & 0 & 0 & 0 & 0 & \alpha & 0 & 0 & 0 & 0 & 0 \\
0 & -\frac{12\beta_z}{L^3} & 0 & 0 & 0 & -\frac{6\beta_z}{L^2} & 0 & \frac{12\beta_z}{L^3} & 0 & 0 & 0 & -\frac{6\beta_z}{L^2} \\
0 & 0 & -\frac{12\beta_y}{L^3} & 0 & \frac{6\beta_y}{L^2} & 0 & 0 & 0 & \frac{12\beta_y}{L^3} & 0 & \frac{6\beta_y}{L^2} & 0 \\
0 & 0 & 0 & -\gamma & 0 & 0 & 0 & 0 & 0 & \gamma & 0 & 0 \\
0 & 0 & -\frac{6\beta_y}{L^2} & 0 & \frac{2\beta_y}{L} & 0 & 0 & 0 & \frac{6\beta_y}{L^2} & 0 & \frac{4\beta_y}{L} & 0 \\
0 & \frac{6\beta_z}{L^2} & 0 & 0 & 0 & \frac{2\beta_z}{L} & 0 & -\frac{6\beta_z}{L^2} & 0 & 0 & 0 & \frac{4\beta_z}{L}
\end{bmatrix} \tag{A5}$$

For the given element, the stiffness and mass sensitivity matrices have the same pattern as $K^{(e)}$ and $M^{(e)}$. Only the coefficients α, β_y, β_z, γ, m_v, and m_θ need to be redefined as follows. Each column of Tables A1 and A2 gives their values for a specific sensitivity matrix.

Appendix B: Algorithm for Establishing a Threshold for an Error Distribution

Let i denote a generic degree of freedom in a given finite element model containing n_{DOF} DOF, and let $ER(i)$ denote the value of some error function ER at the ith DOF in that model. The problem here is to find a threshold l such that the DOF where $ER(i) \geq l$ captures the "essence" of the error ER. We refer to these DOF as the retained DOF. If the indices i are sorted such that

$$i<j \Rightarrow ER(i)>ER(j) \tag{B1}$$

then $ER(1)$ becomes the largest error $ER^{\max}$ (Fig. B1). The total error in the model is

$$ER^{\text{total}} = \mathfrak{A} = \sum_{i=1}^{i=n_{\text{DOF}}} ER(i) \tag{B2}$$

and is graphically represented by the area between the curve $ER(i)$ and the horizontal axis. For a uniform error distribution $ER(i) = ER(1)$, this area becomes $\mathfrak{A}^* = ER(1)\times n_{\text{DOF}}$ and is graphically represented by the area of the rectangle outlined in Fig. B1. We construct a threshold l as follows:

$$l = ER([s\times(\mathfrak{A}/\mathfrak{A}^*)\times n_{\text{DOF}}]) \tag{B3}$$

where [ ] denotes the operator that identifies an input quantity with its closest integer value, and s is a user-defined "shrinking" parameter which varies between 0 and 1 depending on the memory and CPU resources that are available to the user. Clearly, l is defined as the error level of a DOF indexed by $j_l = [s\times(\mathfrak{A}/\mathfrak{A}^*)\times n_{\text{DOF}}]$. The ratio j_l/n_{DOF} represents the percentage of DOF that should be retained to capture most of the global error and is identified with the ratio $\mathfrak{A}/\mathfrak{A}^*$. The reason behind this identification is as follows. Suppose that s is set to 1 and consider the two extreme cases of error distribution: 1) a uniform error distribution and 2) a localized one (Fig. B1). In the first case, one should retain all DOF, and that is correctly predicted by $j_l = (\mathfrak{A}/\mathfrak{A}^*)\times n_{\text{DOF}} \approx n_{\text{DOF}}$. In the second case, one should retain only the few DOF where the error is concentrated, and that is also correctly predicted by $j_l = (\mathfrak{A}/$

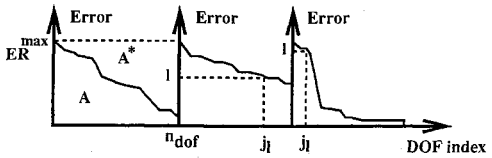

Fig. B1 Three sorted error distributions: generic, uniform, and localized.

$\mathcal{C}^*) \times n_{DOF} \ll n_{DOF}$ since in that case $\mathcal{C} \ll \mathcal{C}^*$. The extra parameter s can be used to reduce the percentage of retained DOF in order to save memory and computational time.

Acknowledgments

The first author would like to acknowledge the support of NASA Headquarters under Grant NAGW-1388. The second author wishes to acknowledge the partial support of the National Science Foundations under Grant ASC-8717773, and the partial support of Aerospatiale, France.

References

[1]Baruch, M., "Optimization Procedure to Correct Stiffness and Flexibility Matrices Using Vibration Tests," *AIAA Journal,* Vol. 16, No. 11, 1978, pp. 1209, 1210.

[2]Berman, A., and Nagy, E. J., "Improvement of a Large Analytical Model Using Test Data," *AIAA Journal,* Vol. 21, No. 8, 1983, pp. 1168–1173.

[3]Caesar, B., "Update and Identification of Dynamic Mathematical Models," *Proceedings of the 1st International Modal Analysis Conference* (Orlando, FL), Society for Experimental Mechanics and Union College, 1983, pp. 394–401.

[4]Kabe, A. M., "Stiffness Matrix Adjustment Using Mode Data," *AIAA Journal,* Vol. 23, No. 9, 1985, pp. 1431–1436.

[5]Smith, S. W., and Beattie, C. A., "Secant-Method Adjustment for Structural Models," *AIAA Journal,* Vol. 29, No. 1, 1991, pp. 119–126.

[6]Chen, J. C., Kuo, C. P., and Garba, J. A., "Direct Structural Parameter Identification by Modal Test Results," *Proceedings of the 24th AIAA/ASME/ASCE/AHS Structures, Structural Dynamics, and Materials Conference,* AIAA, New York, 1983, pp. 44–49.

[7]Collins, J. D., Hart, G. C., Hasselman, T. K., and Kennedy, B., "Statistical Identification of Structures," *AIAA Journal,* Vol. 12, No. 2, 1974, pp. 185–190.

[8]Chen, J. C., and Wada, B. K., "Criteria for Analysis-Test Correlation of Structural Dynamics Systems," *Journal of Applied Mechanics,* Vol. 42, No. 4, 1975, pp. 471–477.

[9]Lallement, G., and Piranda, D., "Localization Methods for Parametric Updating of FE Models," *Proceedings of the 8th International Modal Analysis Conference* (Kissimmee, FL), Society for Experimental Mechanics and Union College, 1990, pp. 579–585.

[10]Lallement, G., and Zhang, Q., "Inverse Sensitivity Based on the Eigensolutions: Analysis of Some Difficulties Encountered in the Problem of Parametric," *Proceedings of the 13th International Modal Analysis Seminar,* edited by K. U. Leuven, K. U. Leuven, Leuven, Belgium, 1988, pp. 1–16.

[11]Berger, H., Chaquin, J. P., and Ohayon, R., "Finite Element Model Adjustment Using Experimental Modal Data," *Proceedings of the 2nd International Modal Analysis Conference,* 1984, pp. 1–5.

[12]Ojalvo, I. U., and Pilon, D., "Diagnostics for Geometrically Locating Structural Math Errors from Modal Test Data," *Proceedings of the 29th AIAA/ASME/ASCE/AHS Structures, Structural Dynamics, and Materials Conference* (Williamsburg, VA), AIAA, Washington, DC, 1988, pp. 1174–1186.

[13]Mottershead, J. E., "Theory for the Estimation of Structural Vibration Parameters from Incomplete Data," *AIAA Journal,* Vol. 28, No. 3, 1990, pp. 559–561.

[14]Creamer, N. G., and Junkins, J. C., "Identification Method for Lightly Damped Structures," *Journal of Guidance, Control, and Dynamics,* Vol. 11, No. 6, 1988, pp. 571–576.

[15]Berger, H., Ohayon, R., Barthe, L., and Chaquin, J. P., "Parametric Updating of FE Model Using Experimental Simulation: A Dynamic Reaction Approach," *Proceedings of the 8th International Modal Analysis Conference* (Kissimmee, FL), Society for Experimental Mechanics and Union College, 1990, pp. 180–186.

[16]Bernitsas, M. M., and Tawekal, R., "Structural Model Correlation Using Large Admissible Perturbations in Cognate Space," *AIAA Journal,* Vol. 29, No. 12, 1991, pp. 2222–2232.

[17]Ibrahim, S. R., and Saafan, A. A., "Correlation of Analysis and Test in Modeling of Structures, Assessment and Review," *Proceedings of the 5th International Modal Analysis Conference* (London), Society for Experimental Mechanics and Union College, 1987, pp. 1651–1660.

[18]Caesar, B., "Update and Identification of Dynamic Mathematical Models," *Proceedings of the 5th International Modal Analysis Conference* (London), Society for Experimental Mechanics and Union College, 1987, pp. 453–459.

[19]Heylen, W., and Sas, P., "Review of Model Optimization Techniques," *Proceedings of the 5th International Modal Analysis Conference* (London), Society for Experimental Mechanics and Union College, 1987, pp. 1177–1182.

[20]Guyan, R. J., "Reduction of Stiffness and Mass Matrices," *AIAA Journal,* Vol. 3, No. 2, 1965, pp. 380–385.

[21]Paz, M., "Dynamic Condensation Method," *AIAA Journal,* Vol. 22, No. 5, 1984, pp. 724–727.

[22]Gysin, H. P., "Comparison of Expansion Methods of FE Modeling Error Localization," *Proceedings of the 8th International Modal Analysis Conference* (Kissimmee, FL), Society for Experimental Mechanics and Union College, 1990, pp. 195–204.

[23]Zimmerman, D. C., and Kaouk, M., "Eigenstructure Assignment Approach for Structural Damage Detection," *AIAA Journal,* Vol. 30, No. 7, 1992, pp. 1848–1855.

[24]Golub, G., and Van Loan, C. F., *Matrix Computations,* Johns Hopkins University Press, 1983, pp. 427–435.

[25]Hager, W. W., *Applied Numerical Linear Algebra,* Prentice-Hall, Englewood Cliffs, NJ, 1988, pp. 243–248.

[26]Chen, J. C., "Evaluation of Spacecraft Modal Test Methods," *Journal of Spacecraft and Rockets,* Vol. 24, No. 1, 1987, pp. 52–62.